Synthesis and electrical conductivity of multilayer silicene

Patrick Vogt, Pierre Capiod, Maxime Berthe, Andrea Resta, Paola de Padova, Thomas Brühne, Guy Le Lay, B. Grandidier

Applied Physics Letters

Synthesis and electrical conductivity of multilayer silicene

Cite as: Appl. Phys. Lett. **104**, 021602 (2014); https://doi.org/10.1063/1.4861857
Submitted: 24 September 2013 • Accepted: 28 December 2013 • Published Online: 14 January 2014

P. Vogt, P. Capiod, M. Berthe, et al.

Synthesis and electrical conductivity of multilayer silicene

P. Vogt,[1,a)] P. Capiod,[2] M. Berthe,[2] A. Resta,[3,b)] P. De Padova,[4] T. Bruhn,[1] G. Le Lay,[3,4,b)] and B. Grandidier[2,a)]
[1]*Technische Universität Berlin, Hardenbergstraße 36, 10623 Berlin, Germany*
[2]*Institut d'Electronique, de Microélectronique et de Nanotechnologies (IEMN), CNRS, UMR 8520 Département ISEN, 41 bd Vauban, 59046 Lille Cedex, France*
[3]*Aix-Marseille University, CNRS-CINaM, Campus de Luminy, Case 913, F-13288 Marseille Cedex 09, France*
[4]*Instituto di Struttura della Materia, Consiglio Nazionale delle Ricerche - ISM, via Fosso del Cavaliere, 00133 Roma, Italy*

(Received 24 September 2013; accepted 28 December 2013; published online 14 January 2014)

The epitaxial growth and the electrical resistance of multilayer silicene on the Ag(111) surface has been investigated. We show that the atomic structure of the first silicene layer differs from the next layers and that the adsorption of Si induces the formation of extended silicene terraces surrounded by step bunching. Thanks to the controlled contact formation between the tips of a multiple probe scanning tunneling microscope and these extended terraces, a low sheet resistance, albeit much higher than the electrical resistance of the underlying silver substrate, has been measured, advocating for the electrical viability of multilayer silicene. © *2014 AIP Publishing LLC*.
[http://dx.doi.org/10.1063/1.4861857]

Silicene, the Si analogue of graphene, has recently extended the short list of existing two-dimensional (2D) atomic crystals.[1] Along with the synthesis on silver,[2–6] silicene was also grown on zirconium diboride[7] and Ir(111)[8] substrates. Contrary to graphene, silicene is a purely synthetic group-IV 2D material, opening a possible way for the creation of other similar materials within this group. Although silicene differs from the planar atomic geometry of graphene, due to a low buckled geometry of the Si atoms in the honeycomb lattice, its band structure has been predicted to resemble that of graphene: the energy-momentum dispersion is linear near the Fermi level.[9,10]

So far, several 2D atomic arrangements have been experimentally found after Si deposition on the Ag(111) surface.[4,5,11,12] Among those Si atomic layers, two have been demonstrated to exhibit compatible properties with respect to free-standing silicene: the (4×4) structure[2] (referring to its periodicity with respect to the Ag(111) surface) and the $(\sqrt{3} \times \sqrt{3})R30°$ structure[3,13] (referring to the silicene unit cell). Both atomic structures consist of honeycomb lattices that differ in the way the atoms are buckled. The measured electronic properties are supporting the interpretation of the charge carriers to resemble the ones of Dirac Fermions.[3,13–15] Although, the nature of the experimentally determined band dispersion has been debated for the (4×4) structure,[6,16] it has been recently explained by a silicene induced electronic hybridized state localized at the silicene/Ag(111) interface,[17] in agreement with the experimental observations. As to the $(\sqrt{3} \times \sqrt{3})R30°$ structure, the observation of electronic standing-wave patterns[3,13] and of a cone-like electronic dispersion[18] provide convincing evidence for the successful formation of silicene. Based on these results, a high carrier group velocity, comparable to the one of graphene, has been deduced from the measurement of the constant of proportionality between energy and momentum. Such a result holds good promise to reach high electron mobility in silicene sheets, a key requirement for the integration of this 2D atomic material into radiofrequency electronic devices.[19,20]

For the demonstration of this applicability of silicene, based on recent results that have shown the growth of Si islands on top of the (4×4) and $(\sqrt{3} \times \sqrt{3})R30°$ structures,[4,11,18] we move a step forward. Here, we report on the growth of silicene stacks, consisting of a few atomic layers, where the lowest (initial) one has the (4×4) structure and all following layers show the $(\sqrt{3} \times \sqrt{3})R30°$ structure. Scanning tunneling microscopy (STM) and scanning electron microscopy (SEM) of the surface morphology reveals a Stranski-Krastanov growth mode, with a motion and redistribution of steps upon Si adsorption. This surface reconstruction favours the formation of mesoscopic silicene layers, which have been subsequently characterized with ultra high vacuum (UHV) transport measurements in four-point measurement configurations. Thanks to the ability of STM to limit the tip-induced stress during the electrical contact formation, the sheet resistance of multilayer silicene has been measured and found to be comparable with the one of multilayer graphene consisting of nanograins.

Sample preparation and all experiments were performed under UHV conditions, allowing the contamination-free epitaxial growth of silicon on single crystal Ag(111) substrates. Clean and well-ordered Ag(111) surfaces were prepared by Ar^+-bombardment (1.5 kV, 5×10^{-5} mbar) and subsequent annealing at ~530 °C for 30 min. The synthesis of silicon adlayers was carried out by evaporating atomic Si onto the clean and well-ordered Ag(111) surface, that was held at 210–220 °C. The whole growth process and the evolution of the Si-adlayer was monitored by low energy electron diffraction (LEED). STM measurements were

[a)]Authors to whom correspondence should be addressed. Electronic addresses: patrick.vogt@tu-berlin.de and bruno.grandidier@isen.iemn.univ-lille1.fr
[b)]Present address: CNRS - PIIM UMR 7345, Aix-Marseille University, Campus de St Jérôme, Avenue Escadrille Normandie-Niémen, F-13397 Marseille Cedex 20, France

performed at room temperature in constant-current mode using either an Omicron VT-STM or a multiprobe STM platform combined with a SEM.[21] The bias values refer to the sample voltage with respect to the STM tip. The measured z-distances were carefully calibrated by measuring single atomic steps on the clean Ag(111) surface.

Figure 1(a) shows a STM image of the (4×4) structure formed on the Ag(111) surface for Si coverage lower than 1 monolayer (ML) deposited at a temperature of 220 °C, in agreement with our previous results.[2] While an increase of the temperature of the silver substrate inevitably causes the formation of other phases,[5,11] we have found that the (4×4) structure can be synthesized as the clearly dominant phase within the temperature range of 200–220 °C. This is seen in the left LEED pattern of Figure 1(b), where analysis of the surface with electron diffraction reveals two types of diffraction spots: the integer spots of the bare silver surface and one-four order spots that correspond to the formation of the (4×4) structure of silicene on silver. Note that the 4×4 symmetry with respect to the Ag(111) surface corresponds to the 3×3 phase related to the unit cell of silicene. From now, we will use this (3×3) notation throughout this manuscript.

Upon further Si deposition on the sample, the LEED pattern changes. As highlighted by the blue circle in Figure 1(b), 1/3,1/3 order spots (with reference to (1×1) silicene) become strong in the right pattern. This observation reflects the emergence of another phase that is consistent with the structure observed in the filled-state STM image (Figure 1(c)). At higher magnification (Figure 1(d)), this structure shows a honeycomb-like arrangement, with a distance of 0.64 nm between the dark centers, based on the line profile of Figure 1(e). Therefore, the lattice vector length of this arrangement is $\sqrt{3}$, meaning that the structure has a $(\sqrt{3} \times \sqrt{3})R30°$ unit cell, in agreement with the LEED pattern. We note that the area showing the $(\sqrt{3} \times \sqrt{3})R30°$ structure is higher by 0.20 nm (± 0.02 nm) in comparison with the terrace having the (3×3) structure as determined by the line profile acquired across the boundary between both silicene structures (inset of Figure 1(c)). Such a height is consistent with the one reported in Refs. 18 and 22, and differs from a silver step-edge of 0.24 nm, measured with the same scanning parameters. Based on the height profiles and the fact that we could never observe the occurrence of the $(\sqrt{3} \times \sqrt{3})R30°$ structure before the formation of the (3×3) structure, we suggest that the layer with the $(\sqrt{3} \times \sqrt{3})R30°$ structure grows on top of the initial silicene layer with the (3×3) structure. We have recently shown that the 2nd layer $(\sqrt{3} \times \sqrt{3})R30°$ structure, prepared under similar growth conditions as described here, exhibits two characteristic bands which are centred at the silicene $\bar{K}$ point and can be assigned to conical π and π^* bands.[15] The π^* band is crossing the Fermi level, meaning that there is no electronic band gap, at variance with what was shown for the initial (3×3) silicene layer. The 2nd layer structure resembles the properties of Dirac fermions with a Fermi velocity of $\sim 0.3\ 10^6\,\mathrm{ms}^{-1}$ and is hence related to a silicene structure.

After the deposition of approximately 1.5 ML of Si onto the previous surface, i.e., a total of ~2 MLs of silicon on top of the first (3×3) silicene layer, the intensity of the 1/3,1/3 order spots in the LEED pattern are much brighter (Figure 2(a), inset), meaning a higher coverage of the surface by the $(\sqrt{3} \times \sqrt{3})R30°$ symmetry. This is also clearly visible in the STM image (Figure 2(a)), where the major part of the surface is covered with terraces having the $(\sqrt{3} \times \sqrt{3})R30°$ structure.

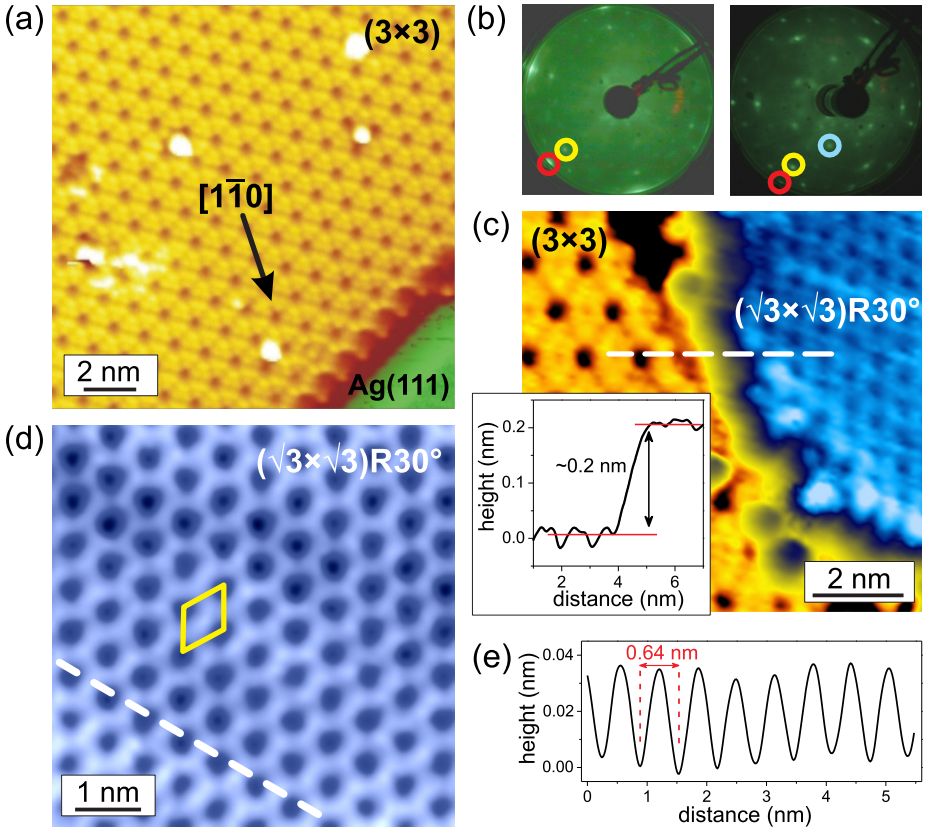

FIG. 1. (a) STM topograph ($U_{bias} = -1.0$ V, $I_t = 1.08$ nA) of (3×3) silicene (yellow area) and bare (1×1) Ag(111) surface (green area). (b) (left) LEED pattern (43 eV) of the submonolayer coverage of Si onto the Ag(111) surface, (right) LEED pattern (46 eV) for a monolayer of Si (red circle: silver integer order spot; yellow circle: silicene integer order spot, blue circles: (1/3,1/3) type superstructure spots of the $(\sqrt{3} \times \sqrt{3})R30°$ silicene). (c) Filled states STM image of the $(\sqrt{3} \times \sqrt{3})R30°$ silicene structure and the initial (3×3) silicene structure for a monolayer of Si ($U_{bias} = -1.1$ V, $I_t = 0.33$ nA). The inset shows a line profile along the dashed line in the STM image. (d) High-resolution STM topographs ($U_{bias} = -1.1$ V, $I_t = 0.65$ nA) of the $(\sqrt{3} \times \sqrt{3})R30°$ silicene structure. The unit cell is indicated by the yellow rhombus. (e) Line profile along the white line indicated in (d).

Only on a small area, the (3×3) silicene structure can still be seen as a 1st layer at the bottom. On top of the (3×3) silicene layer, the formation of 3 terraces incontrovertibly shows the atomic arrangement for the $(\sqrt{3} \times \sqrt{3})R30°$ structure. The single terraces are well-ordered and have clear defined edges. On the top layer, a rather small $(\sqrt{3} \times \sqrt{3})R30°$ island is visible with a diameter of only ~5 nm, indicating the starting point of the next terrace formation. From the line profile in Figure 2(b), recorded along the dashed white line in Figure 2(a), it can be seen that this top island (bright blue) is separated from the layer underneath (dark blue) by ~0.3 nm (±0.02 nm) and the following next layer (green) by ~0.59 nm (±0.02 nm), indicating a single and double atomic step, respectively. These results show that the natural separation between two $(\sqrt{3} \times \sqrt{3})R30°$ layers is 0.3 nm, which corresponds to a one-atom-thick silicene layer. Thus, the total step heights correspond to multiple integers of 0.3 nm. These steps cannot be attributed to possibly underlying steps on the Ag substrate. If this was the case, the step height would correspond to a single Ag step, having a much smaller value of only 0.24 nm. Note also that the top island (bright blue) cannot stem from an underlying Ag step due to its size and form. Finally, the step heights between the $(\sqrt{3} \times \sqrt{3})R30°$ terraces is remarkably larger than the step height of the first $(\sqrt{3} \times \sqrt{3})R30°$ layer on the initial (3×3) silicene of apparently only 0.2 nm. We attribute the difference to an underestimation of the latter due to a different DOS of the (3×3), which is still influenced by the Ag(111) substrate underneath.

With increasing silicon coverage, these layers continue to pile up as shown in Figure 2(c), recorded after a total deposition amount of approximately 5 ML of Si on the (3×3) silicene layer. The single terraces appear flat and well ordered and high-resolution STM images reveal that the clear majority of the terraces show the $(\sqrt{3} \times \sqrt{3})R30°$ structure (indicated as $\sqrt{3}$). The line profiles recorded along the white dashed lines in this image (Figure 2(d)) shows that dominantly single-atomic steps (red arrow) are formed, occasionally accompanied by double- (blue arrow) and triple- (green arrow) atomic steps (Figure 2(d)). Few (3×3) silicene terraces still remain, such as the two adjacent terraces seen in Figure 2(c). We note that both terraces are separated by a value corresponding to the silver step height, whereas the separation with the next layer, which shows a $(\sqrt{3} \times \sqrt{3})R30°$ structure, readily differs and is consistent with the value measured above. Therefore, the STM images demonstrate that multilayer silicene is grown upon Si deposition on an initial silicene layer formed directly on the Ag(111) substrate.

In order to measure the electrical conductivity of multilayer silicene, we further investigated the surface morphology

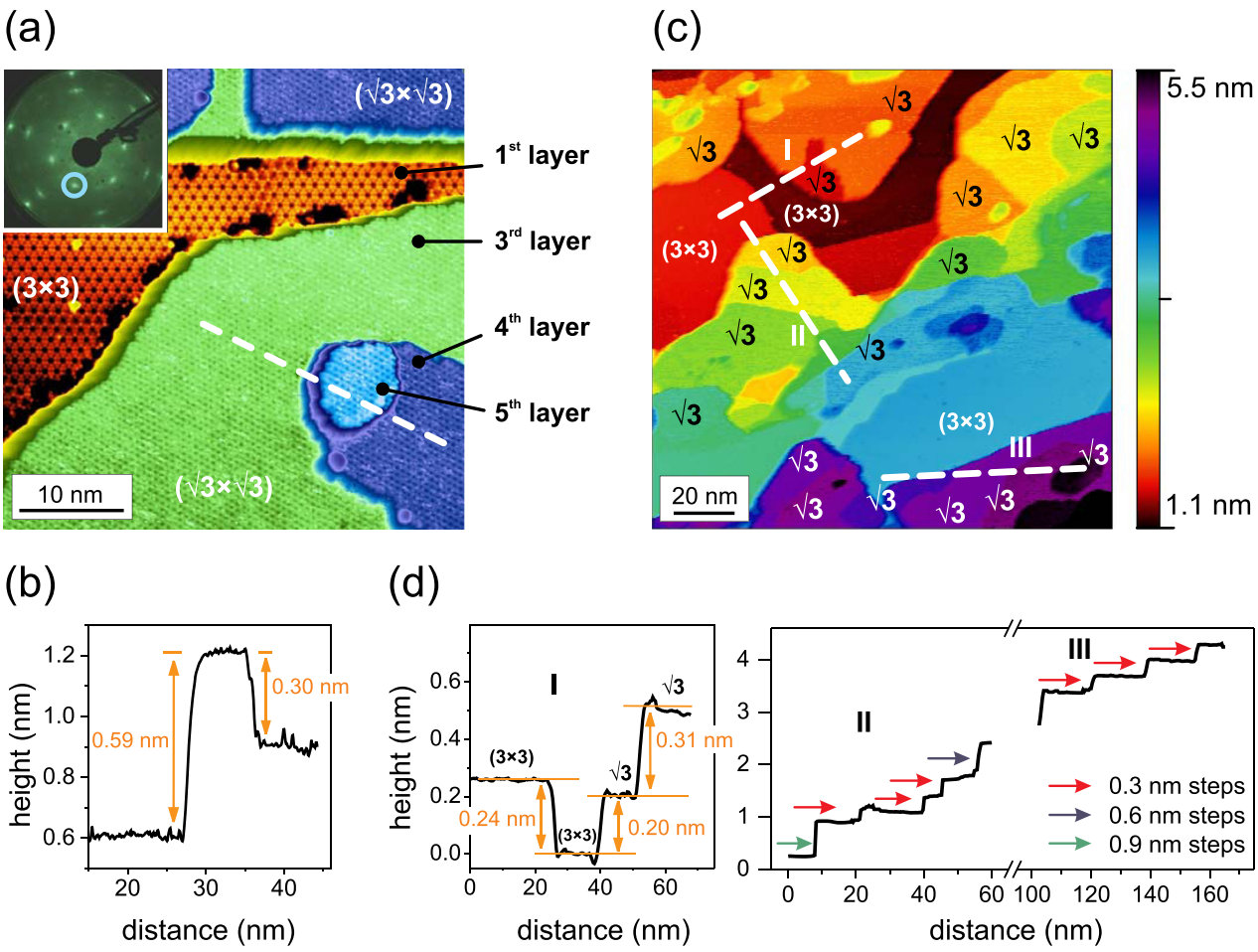

FIG. 2. (a) STM topograph ($U_{bias} = -1.1$ V, $I_t = 0.54$ nA), after deposition of approximately 1.5 ML of Si onto the (3×3) silicene. 3 well-ordered terraces can be seen showing the $(\sqrt{3} \times \sqrt{3})R30°$ arrangement. The 1st (3×3) silicene layer is still visible at the bottom. Inset: LEED pattern of the surface where the (1/3,1/3) type superstructure spots of the $(\sqrt{3} \times \sqrt{3})R30°$ silicene are circled in blue. (b) Line profile along the white line in (a). (c) STM topograph ($U_{bias} = -1.1$ V, $I_t = 1.73$ nA), after deposition of approximately 5 MLs of Si onto the (3×3) silicene layer. (d) Line profile along the white lines (indicated as I, II, and III) in (c).

at the micrometer scale. Starting with the observation of the bare silver surface with SEM, we noted the occurrence of featureless areas that were surrounded with rounded step bunches. These step bunches appear as faint bright lines in Figure 3(a). After the deposition of silicon atoms to obtain the (3×3) phase, the contrast in these areas changes (Figure 3(b)). The step bunches are better resolved and they define a central area, that is decorated with alternating bright and dark rounded stripes. At higher Si coverage, when the 1/3,1/3 order silicene spots are dominant in the LEED pattern, we still see the same shape, but can notice two changes (Figure 3(c)). First, the steps seem to be repelled from the central region, leading to more pronounced step bunches at the boundary. Then, the contrast in the central region is weaker, suggesting a smaller corrugation. It is known that the adsorption of different chemical elements on a clean and well-ordered surface can lead to a morphological change due to the modification of the surface free energy, a change of the surface stress or a modification of the step energy. Such modifications have been investigated when metals are adsorbed on Si surfaces,[23,24] and have also been found after the adsorption of molecules on silver surfaces.[25,26] We thus believe that the adsorption of Si favours the retreat of substrate steps when the edge of the growing lowest silicene layers advances on the silver terraces. It leads to a step rearrangement, where the formation of terraces causes a stronger step bunching in their vicinity. Imaging the centre of the circular shapes with STM (Figure 3(d)) shows a morphology that differs from the typical one observed in Figure 2(c). In agreement with a Stranski-Krastanov growth mode, the top layers now form islands grown on atomically flat silicene layers. One of this flat layer is seen to extend over the whole STM image (width of 180 nm), suggesting the formation of extended silicene layers.

By randomly contacting the multilayer silicene with four STM tips placed in a square arrangement with side length between 1 and 4 μm, we were generally not able to measure a substantial resistance. However, in the regions that show a strong step rearrangement, as seen in Fig. 3, a significant and reproducible voltage drop between two adjacent tips was measured, when a current was passed between the two other tips. For a potential probe separation of 2 μm, the linear extrapolation of the V(I) curves yields resistance values of (i) 727 Ω, (ii) 608 Ω, and (iii) 823 Ω, as shown in Figure 3(f). We point out that such a range of resistances strongly differs from the resistance measured when the multilayer is under strong compression. In that case (see curve (iv) in Figure 3(f)), the voltage drop reaches zero, consistent with a current passing in the Ag substrate. The latter measurement is also in agreement with the meaningless voltage drop measured when the bare Ag support is probed and indicates that the multilayer is electronically decoupled from the silver substrate. In addition, tunnelling spectroscopic measurements support a weak interlayer coupling in the multilayer, as shown by the reduction of the slope in the I(V) curves obtained on the 3rd, 4th, and 5th layers with identical feedback conditions ($U_{bias} = -1.8$ V, $I_t = 1$ nA). Since the separation between the STM tip and the top layer in tunnelling regime is expected to decrease with a higher number of stacked layers when the set-point current is kept constant, an increase of the resistance by an amount of a few tens of GΩ is consistent with a smaller tunnelling probability due to additional tunnelling barriers in series, as found for multiwall nanotubes and bilayer graphene.[27,28] Therefore, the resistance between the sheets is much higher than the resistance of a sheet and conduction occurs only in the highest extended sheet.

Transport measurements were further performed for different probe separations. When the contact leads defined a square with sides several times smaller than the size of the silicene layer, the sheet resistance can be expressed as $R_S = (2\pi/\ln 2)R$, where R is the measured resistance and $2\pi/\ln 2$ the correction factor.[29] We thus applied this formula for a tip spacing of 1 μm and find a sheet resistance of 6.5 kΩ/□. This value is an order of magnitude higher than the typical sheet resistance obtained for uniform multilayer graphene,[30,31] but it is close to the one measured for graphite

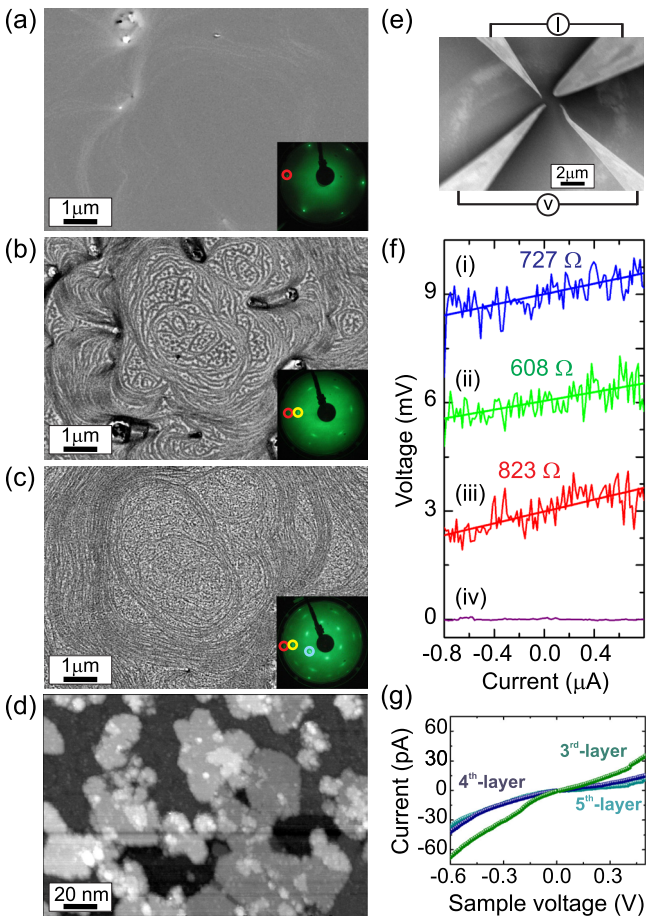

FIG. 3. Left: Evolution of the surface morphology as a function of the Si coverage on the Ag(111) surface observed by SEM: (a) the bare silver surface, (b) the silver surface with a Si coverage <1 ML, and (c) the silver surface with a Si coverage >1 ML. The LEED patterns (insets) recorded at 51 eV, show integer spots for the (1×1) Ag(111) surface (red circle), integer order spots for the (3×3) phase of the 1st silicene layer (yellow circle) and 1/3 order spots for the $(\sqrt{3} \times \sqrt{3})$R30° phase of the next silicene layers (blue circle). (d) STM image ($U_{bias} = 0.7$ V, $I_t = 100$ pA) obtained on a surface similar to (c). Right: Transport measurements of multilayer silicene: (e) SEM image of multilayer silicene being contacted with four W tips in a region of the silver substrate surrounded by a blurred grey contour, corresponding to large step bunches. (f) Set of V-I curves measured on the multilayer silicene with a square arrangement of the four probes. All the curves have been shifted for clarity. Curve (iv) highlights the occurrence of a short circuit by the Ag(111) surface due to the stronger compression of the multilayer with the STM tips. (g) I(V) curves measured with scanning tunnelling spectroscopy on three adjacent layers showing the $(\sqrt{3} \times \sqrt{3})$R30° structure ($U_{bias} = -1.8$ V, $I_t = 1$ nA).

thin films consisting of nanograins.[32] As the spacing between the tip increases, we find a decrease of the resistance ($719 \pm 107\ \Omega$ at 1 μm, $676 \pm 145\ \Omega$ at 2 μm, and $224 \pm 48\ \Omega$ at 4 μm), that is still much higher than the zero resistance obtained for the bare silver surface, thus excluding current leakages towards the Ag substrate. Such a trend is consistent with a higher number of effective pathways for the current in the multilayer, as the numerous pin holes or islands observed in the multilayer certainly affect the electrical conduction.

In conclusion, our results demonstrate that multilayer silicene can be grown epitaxially upon Si deposition on an initial (3×3) silicene layer formed directly on a Ag(111) substrate. Each subsequent silicene layer shows a $(\sqrt{3} \times \sqrt{3})$R30° symmetry. Successful transport measurements, free of short-circuit paths through the Ag support, show a metallic behavior. Although the sheet resistance of silicene is still higher than the one found in high quality multilayer graphene, the perspective to grow mesoscopic silicene sheets in a more controlled fashion makes its use quite promising in electronic applications.

This work was financially supported by the Deutsche Forschungsgemeinschaft (DFG) under Grant No. VO1261/3-1, the EQUIPEX program Excelsior, the CNRS through the DEFI G3N, Renatech, the project 2D-NANOLATTICES of the EU 7th framework program (EU-FP7 FET grant number 270749) and the Project for International Scientific Cooperation (PICS) under grant number 40237. We thank Alain Ranguis for the excellent technical assistance.

[1]M. Xu, T. Liang, M. Shi, and H. Chen, Chem. Rev. **113**, 3766 (2013).
[2]P. Vogt, P. De Padova, C. Quaresima, J. Avila, E. Frantzeskakis, M. C. Asensio, A. Resta, B. Ealet, and G. Le Lay, Phys. Rev. Lett. **108**, 155501 (2012).
[3]L. Chen, C.-C. Liu, B. Feng, X. He, P. Cheng, Z. Ding, S. Meng, Y. Yao, and K. Wu, Phys. Rev. Lett. **109**, 056804 (2012).
[4]B. Feng, Z. Ding, S. Meng, Y. Yao, X. He, P. Cheng, L. Chen, and K. Wu, Nano. Lett. **12**, 3507 (2012).
[5]D. Chiappe, C. Grazianetti, G. Tallarida, M. Fanciulli, and A. Molle, Adv. Mater. **24**, 5088 (2012).
[6]C.-L. Lin, R. Arafune, K. Kawahara, M. Kanno, N. Tsukahara, E. Minamitani, Y. Kim, M. Kawai, and N. Takagi, Phys. Rev. Lett. **110**, 076801 (2013).
[7]A. Fleurence, R. Friedlein, T. Ozaki, H. Kawai, Y. Wang, and Y. Yamada-Takamura, Phys. Rev. Lett. **108**, 245501 (2012).
[8]L. Meng, Y. Wang, L. Zhang, S. Du, R. Wu, L. Li, Y. Zhang, G. Li, H. Zhou, W. A. Hofer, and H.-J. Gao, Nano Lett. **13**, 685 (2013).
[9]C.-C. Liu, W. Feng, and Y. Yao, Phys. Rev. Lett. **107**, 076802 (2011).
[10]M. Ezawa, Phys. Rev. Lett. **109**, 055502 (2012).
[11]R. Arafune, C.-L. Lin, K. Kawahara, N. Tsukahara, E. Minamitani, Y. Kim, N. Takagi, and M. Kawai, Surf. Sci. **608**, 297 (2013).
[12]H. Jamgotchian, Y. Colignon, N. Hamzaoui, B. Ealet, J. Y. Hoarau, B. Aufray, and J. P. Bibérian, J. Phys.: Condens. Matter **24**, 172001 (2012).
[13]L. Chen, H. Li, B. Feng, Z. Ding, J. Qui, P. Cheng, K. Wu, and S. Meng, Phys. Rev. Lett. **110**, 085504 (2013).
[14]J. Avila, P. De Padova, S. Cho, I. Colambo, S. Lorcy, C. Quaresima, P. Vogt, A. Resta, G. Le Lay, and M. C. Asensio, J. Phys.: Condens. Matter **25**, 262001 (2013).
[15]P. De Padova, J. Avila, A. Resta, I. Razado-Colambo, C. Quaresima, C. Ottaviani, B. Olivieri, T. Bruhn, P. Vogt, M. C. Asensio, and G. Le Lay, J. Phys.: Condens. Matter **25**, 382202 (2013).
[16]S. Huang, W. Kang, and L. Yang, Appl. Phys. Lett. **102**, 133106 (2013); Z.-X. Guo, S. Furuya, J.-I. Iwata, and A. Oshiyama, J. Phys. Soc. Jpn. **82**, 063714 (2013); P. Gori, O. Pulci, F. Ronci, S. Colonna, and F. Bechstedt, J. Appl. Phys. **114**, 113710 (2013).
[17]S. Cahangirov, M. Audiffred, P. Tang, A. Iacomino, W. Duan, G. Merino, and A. Rubio, Phys. Rev. B **88**, 035432 (2013).
[18]P. De Padova, P. Vogt, A. Resta, J. Avila, I. Razado-Colambo, C. Quaresima, C. Ottaviano, B. Olivieri, T. Bruhn, T. Hirahara, T. Shirai, S. Hasegawa, M. C. Asensio, and G. Le Lay, Appl. Phys. Lett. **102**, 163106 (2013).
[19]C. Sire, F. Ardiaca, S. Lepilliet, J.-W. T. Seo, M. C. Hersam, G. Dambrine, H. Happy, and V. Derycke, Nano Lett. **12**, 1184 (2012).
[20]Y.-M. Lin, C. Dimitrakopoulos, K. A. Jenkins, D. B. Farmer, H.-Y. Chiu, A. Grill, and Ph. Avouris, Science **327**, 662 (2010).
[21]M. Berthe, C. Durand, T. Xu, J. P. Nys, P. Caroff, and B. Grandidier, in *Title of the Book: Atomic Scale Interconnection Machines*, edited by C. Joachim (Springer, 2012).
[22]A. Resta, T. Léoni, C. Barth, A. Ranguis, C. Becker, T. Bruhn, P. Vogt, and G. Le Lay, Sci. Rep. **3**, 02399 (2013).
[23]K. Yagi, H. Minoda, and M. Degawa, Surf. Sci. Rep. **43**, 45 (2001).
[24]H. Minoda, T. Shimakura, K. Yagi, F.-J. Meyer zu Heringdorf, and M. Horn von Hoegen, Phys. Rev. B **61**, 5672 (2000).
[25]T. David, J. K. Gimzewski, D. Purdie, B. Reihl, and R. R. Schlitter, Phys. Rev. B **50**, 5810 (1994).
[26]K. Glöcker, C. Seidel, A. Soukopp, M. Sokolowski, E. Umbach, M. Böhringer, R. Berndt, and W.-D. Schneider, Surf. Sci. **405**, 1 (1998).
[27]B. Bourlon, C. Miko, L. Forró, D. C. Glattli, and A. Bachtold, Phys. Rev. Lett. **93**, 176806 (2004).
[28]P. W. Sutter, J.-I. Flege, and E. A. Sutter, Nature Mater. **7**, 406 (2008).
[29]L. J. Swartzendruber, Solid-State Electron. **7**, 413 (1964).
[30]C. Mattevi, H. Kim, and M. A. Chhowalla, J. Mater. Chem. **21**, 3324 (2011).
[31]W. Cai, Y. Zhu, X. Li, R. D. Piner, and R. S. Ruoff, Appl. Phys. Lett. **95**, 123115 (2009).
[32]Y. Miyasaka, A. Nakamura, and J. Temmyo, Jpn. J. Appl. Phys., Part 1 **50**, 04DH12 (2011).